Communication

Dual-Polarized Crossed Slot Array Antenna Designed on a Single Laminate for Millimeter-Wave Applications

Qingling Yang, Steven Gao, Qi Luo, Lehu Wen, Yong-Ling Ban, Xuexia Yang, Xiaofei Ren, and Jian Wu

***Abstract*— A novel dual-polarized crossed slot planar array antenna is presented in this communication. The proposed design integrates the antenna array with the feeding networks on a single laminate. The antenna element is developed by using a TE_{210} and TE_{120} mode cavity, which is constructed by inserting a number of metalized posts around the crossed region of two perpendicular substrate integrated waveguides (SIWs). The crossed slot is etched over the cavity and is excited from two orthogonal directions to realize dual-polarization. Owing to the orthogonality between the TE_{210} and TE_{120} mode, high isolation and low cross-polarization are achieved. A prototype of the designed antenna array operating at 25 GHz is fabricated and measured. The measured results confirm that the presented array antenna has high port isolation (>41 dB), high cross-polarization discrimination (XPD) (>26 dB), and high aperture efficiency (40%). With the advantages of simple configuration, good radiation performance, and easy fabrication, this proposed array antenna is a good candidate for millimeter-wave wireless systems.**

***Index Terms*— Dual-polarized antenna, planar array, slot antenna, substrate integrated waveguide (SIW) cavity.**

I. Introduction

Dual-polarized antennas are highly desirable in modern wireless systems since they can combat multipath fading and improve channel capacity [1]. In recent years, millimeter waves (mmWaves) wireless systems have received many interests with benefits such as large bandwidth, high resolution, and small size [2]. However, it is challenging to realize dual-polarized antenna arrays working in mmWave frequency bands. One of the key constraints is that there are limited types of dual-polarized antennas suitable for integrating with feeding networks [3]–[17]. For instance, although the microstrip antenna reported in [3] operates with dual-polarization, it is only used to design a linear array. This is because the feeding networks are interleaved with the antenna elements so that grating lobes will appear if a planar antenna array is realized by using this antenna element. In addition, the dual-polarized mmWave antenna arrays with a large number of elements are very intricate as each polarization requires an independent feeding network. The slot antenna arrays reported in [10] and [11] can provide dual-polarization while being integrated with the feeding networks on a single laminate, but the orthogonally polarized antenna elements in these antenna arrays are separated in different rows. As a result, these antenna arrays have a relatively large aperture size and high cross-polarization level. Thus, in order to achieve high compactness and avoid intersections between feeding networks, many dual-polarized antenna arrays are realized by using multiple laminates [12]–[16]. However, compared with the antenna arrays designed on a single laminate, these antenna arrays have higher design complexity and insertion loss. Besides, the milling technique is used to fabricate the dual-polarized array antennas [14]–[16], yet the fabricated antenna prototypes are bulky and expensive.

The objective of this communication is to design a dual-polarized array antenna with simple geometry and good performance. We develop a novel planar dual-polarized crossed slot frequency-scanning antenna array that can be integrated with the feeding networks on a single laminate. An SIW cavity supporting TE_{210} and TE_{120} modes is employed in designing the antenna element. Different from the conventional TE_{210} or TE_{120} mode cavities shaped by metalized walls with a closed form [18], [19], this cavity is constructed by inserting a number of metalized posts around the crossed region of two perpendicular SIWs. The crossed slot etched over the cavity is excited from orthogonal directions to generate dual-polarization. High port isolation, high aperture efficiency, and high XPD are obtained in the designed antenna array. Furthermore, the antenna has three additional advantages: 1) it is realized on a single laminate with low cost; 2) it is scalable; and 3) it is highly compact and can be easily integrated with front ends.

II. Geometry of the Antenna Array

The layout of the proposed dual-polarized array antenna is illustrated in Fig. 1. In this design, Rogers RT/duroid 5880 laminate with thickness of 0.508 mm, $\epsilon_r = 2.2$ and $\tan\delta = 0.0009$ is used. The antenna array aperture consists of 10×10 dual-polarized antenna elements. Four feeding ports with SIW-to-GCPW (grounded co-planar waveguide) transitions connected to a ten-way equal splitter are used to excite the antenna array. Since each antenna element has high isolation between two orthogonal ports, the full planar array antenna can be considered as ten linear antenna arrays placed in parallel. The number of antenna elements in each column and row is set to $n = 10$. The total radiated power P_{rad} for each linear array is assumed to be $0.95P_0$, where P_0 is the input power. The radiation efficiency of each antenna element is assumed to be η. Thus, the radiation power P_{i_rad} $(i = 1, 2, \ldots, n)$ of the ith antenna element in each column or row is

$$P_{i\_rad} = \eta(1-\eta)^{i-1}P_0. \tag{1}$$

Therefore, the radiated power P_{rad} of each linear antenna array is

$$P_{rad} = \sum_{i=1}^{n} P_{i\_rad} = \sum_{i=1}^{n} \eta(1-\eta)^{i-1}P_0 = 0.95P_0. \tag{2}$$

Manuscript received April 11, 2019; revised September 20, 2019; accepted October 15, 2019. Date of publication November 28, 2019; date of current version May 5, 2020. This work was supported by the China Research Institute of Radiowave Propagation, Engineering and Physical Sciences Research Council (EPSRC), under Grant EP/P015840/1, Grant EP/N032497/1, and Grant EP/S005625/1. *(Corresponding author: Qingling Yang.)*

Q. Yang, S. Gao, Q. Luo, and L. Wen are with the School of Engineering and Digital Arts, University of Kent, Canterbury CT2 7NZ, U.K. (e-mail: qy31@kent.ac.uk).

Y.-L. Ban is with the School of Electronic Science and Engineering, University of Electronic Science and Technology of China, Chengdu 611731, China.

X. Yang is with the School of Communication and Information Engineering, Shanghai University, Shanghai 200444, China.

X. Ren and J. Wu are with the China Research Institute of Radiowave Propagation, Xinxiang 453003, China.

Color versions of one or more of the figures in this communication are available online at http://ieeexplore.ieee.org.

Digital Object Identifier 10.1109/TAP.2019.2952244

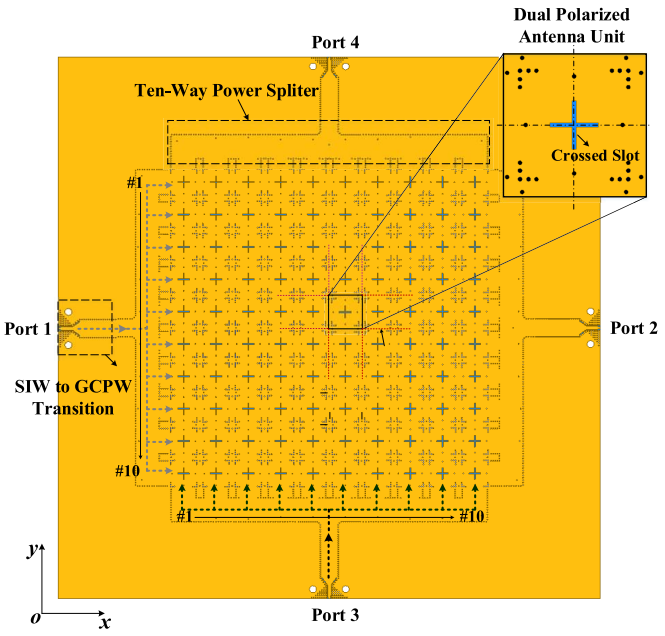

Fig. 1. Layout of the proposed dual-polarized crossed slot planar antenna array.

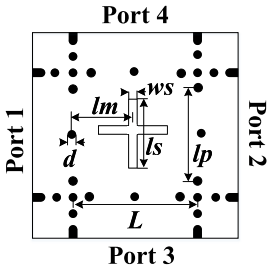

Fig. 2. Layout of the antenna element. Detailed dimensions are $l_m = 3.48$ mm, $d = 0.3$ mm, $w_s = 0.3$ mm, $l_s = 3$ mm, $l_p = 5$ mm, and $L = 7$ mm.

By solving (2), the desired radiation efficiency of each antenna element is calculated to be 26%. In our design, the antenna element can be regarded as a four-port network. Thus, the radiation efficiency of each element is obtained from the S-parameters of the four-port network [4], which is expressed as

$$\eta = \frac{1 - |S_{11}|^2 - |S_{21}|^2 - |S_{31}|^2 - |S_{41}|^2}{1 - |S_{11}|^2} \times 100\%. \quad (3)$$

In this formula, the ohmic losses are not taken into account. Be noted that the dielectric losses are included in (3) because the S-parameters are obtained from the HFSS simulations where the dielectric losses of Rogers RT/duroid 5880 laminate are considered.

III. Antenna Element and Antenna Array Design

A. Dual-Polarized Antenna Element

Fig. 2 shows the configuration of the developed dual-polarized antenna element. It consists of a crossed slot over a cavity supporting TE_{210} and TE_{120} modes. The cavity is formed by a number of metalized posts. Four of these posts are located along the center line and the rest are placed around the corners. The dominant frequency f_0 in a square TE_{210} or TE_{120} mode cavity is [20]

$$f_0 \approx \frac{\sqrt{5}c_0}{2L\sqrt{\epsilon_r}} \quad (4)$$

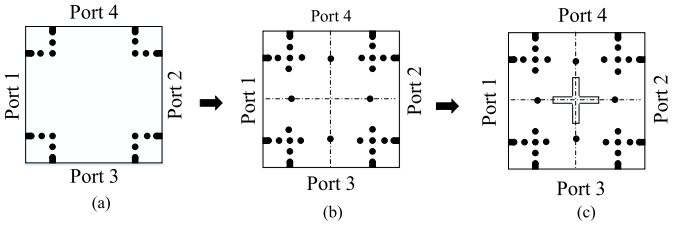

Fig. 3. Design process of the antenna element. (a) Two perpendicular SIWs. (b) TE_{210} and TE_{120} mode cavity. (c) Proposed antenna element.

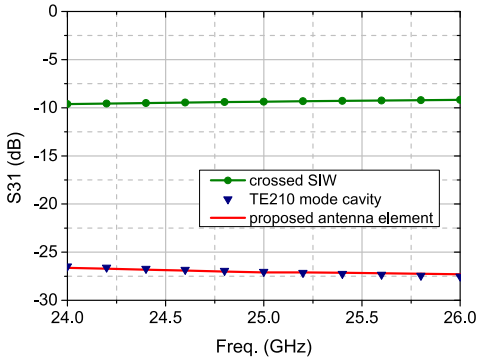

Fig. 4. Simulated S_{31} for three different structures.

where c_0 is the velocity of waves traveling in free-space, ϵ_r is the relative permittivity of the laminate, and L is the side length of the square cavity. It is worth mentioning that (4) is exact for fully enclosed cavity. Therefore, the synthesized cavity size L should be smaller than the theoretical one. The proposed antenna element operates with horizontal polarization by exciting Port 1 or Port 2, and in this case, Port 3 and Port 4 are isolated. Vertical polarization is achieved by exciting Port 3 or Port 4, while Port 1 and Port 2 are isolated correspondingly.

B. Antenna Design

To illustrate the design process of the proposed antenna element, the reference structures are shown in Fig. 3. As shown in Fig. 3(a), the proposed antenna is developed from a crossed SIW where two SIWs are perpendicular to each other with an open region. In Fig. 3(b), a number of metalized posts are inserted around the crossed region to form a TE_{210} and TE_{120} mode cavity. Four of these metalized posts are placed along the centerlines, and the rest of them are located around the corners. As shown in Fig. 3(c), the proposed antenna is realized by etching a crossed slot over the cavity. Fig. 4 shows the simulated S_{31} of the reference structures in the design process. In the crossed SIW, strong coupling higher than -10 dB in the band 24–26 GHz is observed between Port 1 and Port 3. The isolation is improved by exciting the TE_{210} and TE_{120} mode of the SIW cavity, which is higher than 26 dB. Thus, the crossed slot etched over the cavity can be excited from two orthogonal directions to realize dual-polarization while maintaining high isolation.

In the proposed antenna, high isolation and high XPD are achieved by the orthogonality between TE_{210} and TE_{120} mode. In order to better illustrate the working principle of the proposed dual-polarized antenna, the field distribution in the reference structures are shown in Fig. 5. From Fig. 5(a), it is observed that the field is distributed at Port 3 and Port 4 when Port 1 is excited. This is because no structures are applied to constrain the field behavior in the open region of the crossed SIW. In the SIW cavity, most of the electric fields are restrained to propagate along the horizontal direction, as shown

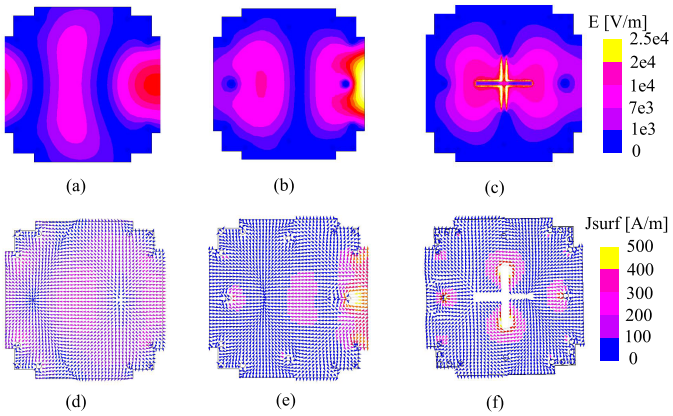

Fig. 5. Field and current distribution. (a)–(c) Electric field distribution in the structures presented in Fig. 3(a), (c), and (d), respectively. (d)–(f) Current distribution in the structures presented in Fig. 3 (a), (c), and (d), respectively.

in Fig. 5(b). However, it should be noted that the TE_{210} mode field distribution in the SIW cavity are not odd symmetric. It results in degraded polarization purity if a slot antenna is designed with such a cavity. To address this issue, it is necessary to introduce an additional perturbation into the cavity. As shown in Fig. 5(c), the presence of the crossed slot affects the electric field distribution inside the cavity. Thus, the crossed slot in this structure acts not only as a dual-polarized radiating element but also a perturbation to improve the symmetry of the TE_{210} mode. In this cavity, the electric fields of the TE_{210} mode have equal magnitude but are out of phase across the center line. The waves are well restrained to propagate along the horizontal direction. When Port 1 is excited, the transverse slot is excited to radiate horizontally polarized waves, because the electric fields on both sides of the transverse slot are out of phase. In addition, as can be seen from Fig. 5(c) and (f), almost no fields are observed at Port 3 and Port 4, indicating that high port isolation is achieved. Similarly, the TE_{120} mode is observed in the cavity when either Port 3 or Port 4 is excited. In this case, the longitudinal slot of this antenna element is excited and radiate vertically polarized waves, while the horizontal ports (Port 1 and Port 2) are well isolated.

For the proposed antenna element, the resonance of the antenna element and the isolation between Port 1 and Port 3 (or Port 4) are mainly affected by the location (l_m) and size (d) of the inserted posts at the center lines. As shown in Fig. 6(a), by increasing l_m, the resonant frequency shifts to the lower frequency band because the effective cavity size is enlarged. The small variation of the reflection coefficients for different l_m indicates that the location of the metalized posts at the center lines mainly affect the resonance while the return loss remains stable at the resonant frequencies. In Fig. 6(b), it is shown that the resonant frequency of the cavity is sensitive to the size of the metalized posts. The resonant frequency is increased by enlarging the post size. As shown in Fig. 6(c) and (d), high port isolation is obtained by increasing l_m and decreasing the size of the inserted metalized posts. The radiation efficiency of the proposed antenna can be tuned by varying the slot width w_s, as shown in Fig. 7. When w_s is increased, the peak efficiency shifts to the lower frequency and is increased.

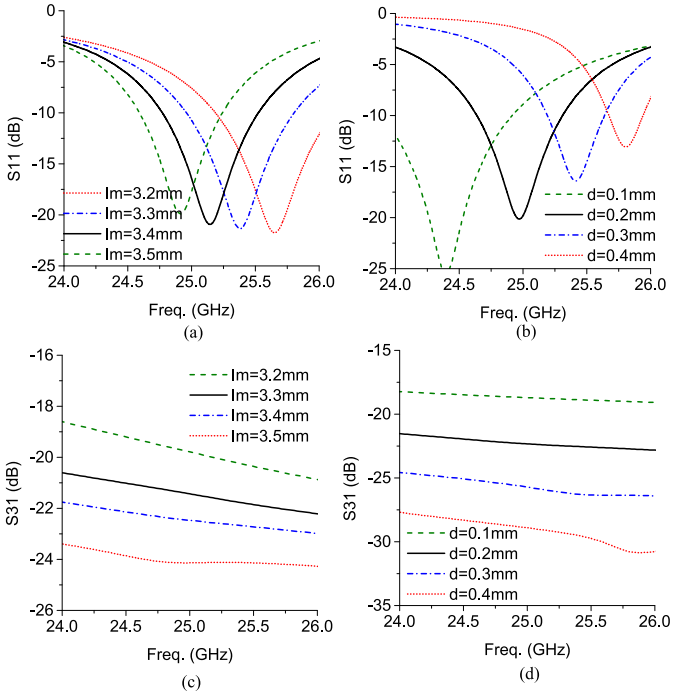

Fig. 6. Parametric study of the effect of different geometrical parameters on the S-parameters. Effects of (a) l_m and (b) d on the S_{11} and effect of (c) l_m and (d) d on the S_{31}.

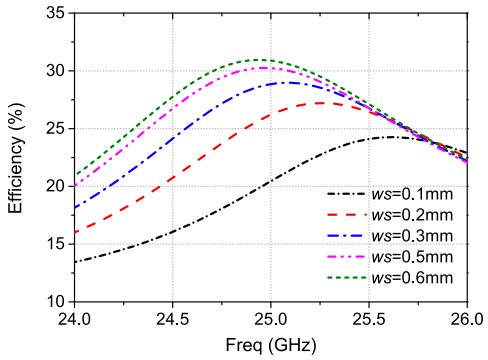

Fig. 7. Effect of w_s on the radiation efficiency.

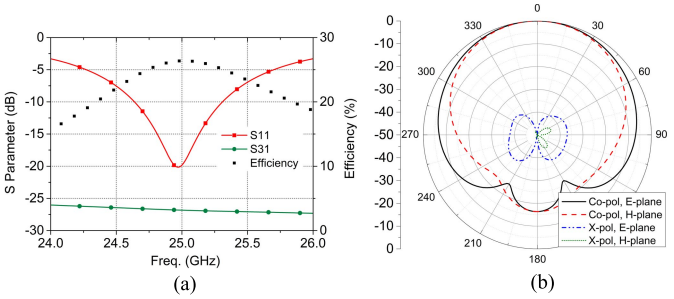

Fig. 8. Simulated performance of the proposed antenna element. (a) S-parameters and radiation efficiency. (b) Normalized radiation patterns.

C. Antenna Element Performance

The optimized dimensions of the developed antenna element are shown in the caption of Fig. 2. Fig. 8(a) shows the simulated S-parameters and radiation efficiency of the designed antenna element. High return loss and high port isolation are achieved. The −10 dB reflection coefficient bandwidth is 700 MHz (24.6–25.3 GHz) and the isolation between Port 1 and Port 3 is higher than 26 dB. The radiation efficiency is 26.3% at the center frequency, which is close to the desired radiation efficiency calculated from (2). Fig. 8(b) presents the simulated radiation patterns of the

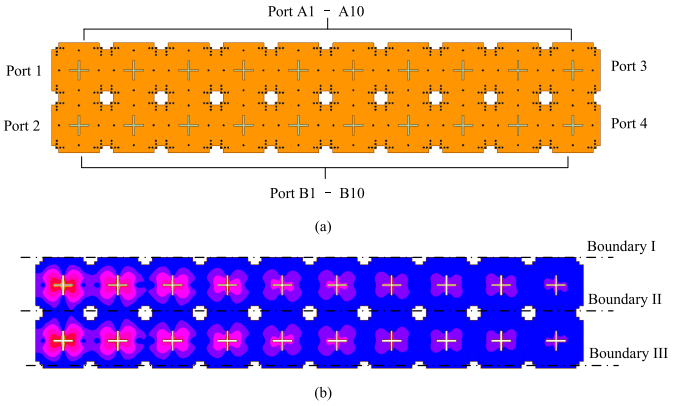

Fig. 9. Subarray formed by two linear antenna arrays. (a) Geometry. (b) Field distribution when Port 1 and Port 2 are excited synchronously.

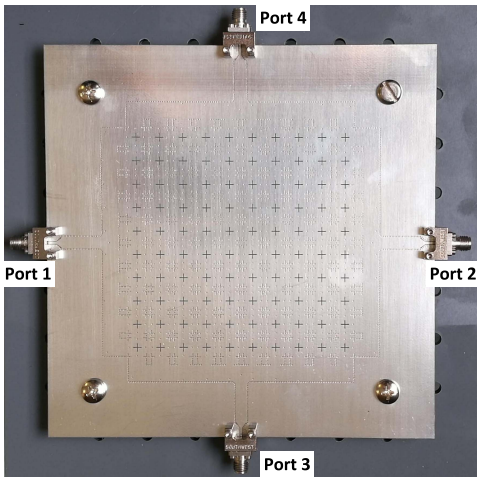

Fig. 10. Fabricated prototype of the array antenna.

antenna element at 25 GHz. Symmetrical patterns are observed in both E-plane and H-plane. In addition, the XPD is higher than 40 dB. This demonstrates that good dual-polarized radiation is realized in the designed antenna element.

D. Subarray

Using the developed antenna element, a subarray composed of two linear antenna arrays is designed and shown in Fig. 9(a). The antenna element spacing is 9.4 mm, which is $0.78\lambda_0$ at 25 GHz. In this subarray, Port 1 and Port 2 are simultaneously excited with uniform amplitude and phase. Port A1–A10 and Port B1–B10 are connected to the subsequent linear arrays. All these ports including Port 3 and Port 4 are terminated with a matched load. Fig. 9(b) shows the simulated electric field distribution of the subarray at 25 GHz. It is observed that at Boundary I, Boundary II, and Boundary III, the fields are reduced to a very weak level. This indicates that the waves in the two linear arrays are bounded by three virtual SIWs. Signals are allowed to independently travel in the two linear arrays with little interference. The electric fields in the substrate are gradually radiated and decayed along each linear array. Similar field distribution can be observed when excitation is from the vertical direction. Thus, the planar antenna array composed of the proposed antenna element is scalable and can be excited from different directions to realize dual-polarization on a single laminate.

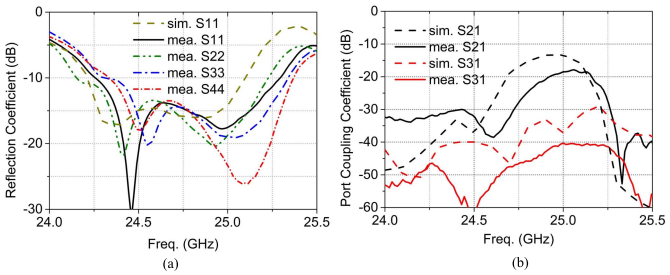

Fig. 11. Simulated and measured S-parameters of the fabricated array antenna. (a) Reflection coefficient. (b) Port coupling level.

IV. Measurement and Discussion

A prototype of the presented dual-polarized antenna array was fabricated and shown in Fig. 10. Its dimension is 157.4 mm × 157.4 mm × 0.508 mm and the antenna array aperture size is 94 mm × 94 mm. Four 2.92 mm end-launch connectors are used to connect the antenna with test equipment. The screws are used to fix the fabricated antenna to the test platform.

A. Return Loss and Isolation

Fig. 11 shows the measured and simulated S-parameters of the fabricated prototype. The measured S_{11} agrees well with the simulated results, as shown in Fig. 11(a). The measured reflection coefficient S_{11} less than −10 dB is from 24.2 to 25.35 GHz. Due to the symmetry of the antenna array, the reflection coefficient at each port is very similar. The overlapped bandwidth for which all the ports are matched below −10 dB is 24.3–25.25 GHz.

The measured and simulated port isolations are shown in Fig. 11(b). The simulated S_{21} is −13 dB which is very close to the designed residual power, $0.05P_0$. Within the bandwidth, the measured transmission loss between Port 1 and Port 2 is lower than the simulated one due to additional loss caused by the connectors. The simulated isolation between Port 1 and Port 3 is larger than 30 dB within the bandwidth, while the measured one is higher than 41 dB.

B. Radiation Pattern

Fig. 12 shows the comparison between the simulated and measured normalized radiation patterns at 24.8, 25, and 25.2 GHz when Port 1 and Port 2 are excited. A good agreement between the simulated and measured results is achieved. The frequency scanning radiation patterns are shown in Fig. 12(a). From 24.8 to 25.2 GHz, a scanning range of 36° is realized, where the beams from −18° to 0° are realized by frequency scanning with Port 1 excited, and scanning range from 0° to 18° are realized with Port 2 excited. The sidelobe levels are less than −9.3 dB over the frequency bandwidth. The −3 dB beamwidth at different frequencies keeps stable, which is with an average of 8°. The overlapped levels between radiation patterns are higher than −2.9 dB. As shown in Fig. 12(b), the cross-polarization keeps in a low level because of high polarization purity and high port isolation in the antenna element. The measured XPD at 25 GHz is larger than 26 dB.

C. Gain and Efficiency

Fig. 13 shows the simulated and measured gain and efficiency of the designed planar array antenna. It shows that the antenna has a high gain from 24.6 to 25.3 GHz. The simulated realized gain is up to 25.7 dBi with a variation of 2.8 dB over the bandwidth.

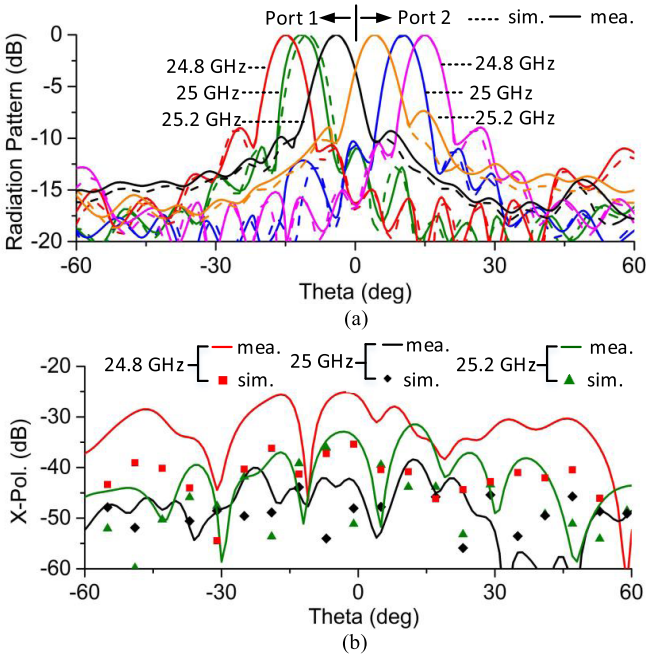

Fig. 12. Radiation patterns. (a) Simulated and measured co-polarization patterns. (b) Simulated and measured XPD patterns.

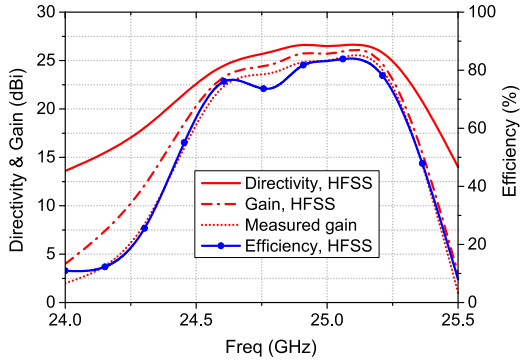

Fig. 13. Directivity, gain, and radiation efficiency.

TABLE I

COMPARISON BETWEEN THIS COMMUNICATION AND THE REPORTED FREQUENCY-SCANNING ARRAY ANTENNAS

Ref.	BW (GHz)	No. Sub.	Scanning Range	Pol.	XPD (dB)	Array Type	$\eta_{ap.}$
[4]	2.7-3.0	3	(70°,88°)	dual	30	linear	14%
[5]	2.4-2.48	1	n.a.	dual	16	planar	11%
[10]	33-39	1	(1°,35°)	dual	18	linear	34%
[21]	8.5-14.1	3	(-17°,52°)	single	n.a.	linear	34%
[22]	8.9-10.6	3	(-28°,46°)	single	n.a.	linear	20%
[23]	13.5-13.9	1	(2°,37°)	single	n.a.	linear	17%
[24]	28-32	2	(4°,20°)	single	27	linear	28%
Proposed	24.8-25.2	1	(-18°,18°)	dual	26	planar	40%

In comparison, the measured gains are about 0.8 dB lower than the simulated ones over the bandwidth. This discrepancy is caused by the connector insertion loss, fabrication tolerance, and uncertainty of dielectric loss. The measured gain has a peak value of 24.9 dBi. The radiation efficiency is larger than 76% from 24.6 to 25.3 GHz, which is calculated from the simulated directivity and gain.

D. Comparison

A comparison between this work and the recently reported frequency-scanning antenna arrays is summarized in Table I. The antenna array in [4] is a dual-polarized frequency-scanning array antenna with high XPD. However, it has a narrow frequency-scanning range and low aperture efficiency. Although the antenna arrays in [5] and [10] provide dual-polarization while being implemented on a single laminate, they are realized by designing the orthogonal antenna elements in separate rows. Hence, the cross-polarization level of these antennas is degraded and their aperture efficiency is limited to 34%. The antenna arrays in [21] and [22] have wide scanning range, but they are limited to single polarization and are difficult to be used in planar arrays. In addition, multiple substrates are needed to realize such array antennas. The antenna arrays in [23] and [24] only provide single polarization and have limited scanning range. As can be seen from Table I, although the proposed antenna array has a relatively narrow impedance bandwidth, it is dual-polarized and can be realized on a single laminate. The frequency scanning range of the proposed antenna array is from $-18°$ to 18°. Besides, it also has advantages of high aperture efficiency (40%) and high XPD (>26 dB) as compared with other reported frequency-scanning array antennas.

V. CONCLUSION

A planar dual-polarized crossed slot array antenna based on a SIW cavity supporting TE_{210} and TE_{120} modes is presented. The antenna array is realized on a single laminate with simple configuration, high integration, and low profile. The 10×10 antenna array operating at 25 GHz is fabricated and measured. The measured port isolation is higher than 41 dB. The measured peak gain is 24.9 dBi and the measured XPD is higher than 26 dB. The aperture efficiency of this array antenna is 40%. The simulated radiation efficiency is higher than 76% within the operation bandwidth. The presented array antenna can be easily integrated with the front ends. Thus, it is a good candidate for wireless communication systems.

REFERENCES

[1] V. Eiceg, H. Sampath, and S. Catreux-Erceg, "Dual-polarization versus single-polarization MIMO channel measurement results and modeling," *IEEE Trans. Wireless Commun.*, vol. 5, no. 1, pp. 28–33, Jan. 2006.

[2] D. Liu, W. Hong, T. S. Rappaport, C. Luxey, and W. Hong, "What will 5G antennas and propagation be?" *IEEE Trans. Antennas Propag.*, vol. 65, no. 12, pp. 6205–6212, Dec. 2017.

[3] G. F. Hamberger, S. Trummer, U. Siart, and T. F. Eibert, "A planar dual-polarized microstrip 1-D-beamforming antenna array for the 24-GHz band," *IEEE Trans. Antennas Propag.*, vol. 65, no. 1, pp. 142–149, Jan. 2017.

[4] S. Karimkashi and G. Zhang, "A dual-polarized series-fed microstrip antenna array with very high polarization purity for weather measurements," *IEEE Trans. Antennas Propag.*, vol. 61, no. 10, pp. 5315–5319, Oct. 2013.

[5] Y. Li, Z. Zhang, C. Deng, Z. Feng, and M. F. Iskander, "2-D planar scalable dual-polarized series-fed slot antenna array using single substrate," *IEEE Trans. Antennas Propag.*, vol. 62, no. 4, pp. 2280–2283, Apr. 2014.

[6] Y. Li and K.-M. Luk, "60-GHz dual-polarized two-dimensional switch-beam wideband antenna array of aperture-coupled magneto-electric dipoles," *IEEE Trans. Antennas Propag.*, vol. 64, no. 2, pp. 554–563, Feb. 2016.

[7] A. Li, K.-M. Luk, and Y. Li, "A dual linearly polarized end-fire antenna array for the 5G applications," *IEEE Access*, vol. 6, pp. 78276–78285, 2018.

[8] L. Schulwitz and A. Mortazawi, "Millimeter-wave dual polarized L-shaped horn antenna for wide-angle phased arrays," *IEEE Trans. Antennas Propag.*, vol. 54, no. 9, pp. 2663–2668, Sep. 2006.

[9] M. Esquius-Morote, M. Mattes, and J. R. Mosig, "Orthomode transducer and dual-polarized horn antenna in substrate integrated technology," *IEEE Trans. Antennas Propag.*, vol. 62, no. 10, pp. 4935–4944, Oct. 2014.

[10] Y. J. Cheng, W. Hong, and K. Wu, "Millimeter-wave half mode substrate integrated waveguide frequency scanning antenna with quadri-polarization," *IEEE Trans. Antennas Propag.*, vol. 58, no. 6, pp. 1848–1855, Jun. 2010.

[11] S. Park, Y. Okajima, J. Hirokawa, and M. Ando, "A slotted post-wall waveguide array with interdigital structure for 45° linear and dual polarization," *IEEE Trans. Antennas Propag.*, vol. 53, no. 9, pp. 2865–2871, Sep. 2005.

[12] J. Xu, W. Hong, Z. H. Jiang, J. Chen, and H. Zhang, "A Q-band low-profile dual circularly polarized array antenna incorporating linearly polarized substrate integrated waveguide-fed patch subarrays," *IEEE Trans. Antennas Propag.*, vol. 65, no. 10, pp. 5200–5210, Oct. 2017.

[13] Z. Chen, H. Liu, J. Yu, and X. Chen, "High gain, broadband and dual-polarized substrate integrated waveguide cavity-backed slot antenna array for 60 GHz band," *IEEE Access*, vol. 6, pp. 31012–31022, 2018.

[14] G.-L. Huang, S.-G. Zhou, T.-H. Chio, C.-Y.-D. Sim, and T.-S. Yeo, "Waveguide-stripline series–corporate hybrid feed technique for dual-polarized antenna array applications," *IEEE Trans. Compon., Packag., Manuf. Technol.*, vol. 7, no. 1, pp. 81–87, Jan. 2017.

[15] X. Lu, H. Zhang, S. Gu, H. Liu, X. Wang, and W. Lu, "A dual-polarized cross-slot antenna array on a parallel-plate waveguide with compact structure and high efficiency," *IEEE Antennas Wireless Propag. Lett.*, vol. 17, pp. 8–11, Jan. 2018.

[16] D. Kim, M. Zhang, J. Hirokawa, and M. Ando, "Design and fabrication of a dual-polarization waveguide slot array antenna with high isolation and high antenna efficiency for the 60 GHz band," *IEEE Trans. Antennas Propag.*, vol. 62, no. 6, pp. 3019–3027, Jun. 2014.

[17] H. Chu and Y.-X. Guo, "A filtering dual-polarized antenna subarray targeting for base stations in millimeter-wave 5G wireless communications," *IEEE Trans. Compon., Packag., Manuf. Technol.*, vol. 7, no. 6, pp. 964–973, May 2017.

[18] J. Xu, Z. N. Chen, X. Qing, and W. Hong, "140-GHz TE_{20}-mode dielectric-loaded SIW slot antenna array in LTCC," *IEEE Trans. Antennas Propag.*, vol. 61, no. 4, pp. 1784–1793, Apr. 2013.

[19] S. A. Winkler, W. Hong, M. Bozzi, and K. Wu, "Polarization rotating frequency selective surface based on substrate integrated waveguide technology," *IEEE Trans. Antennas Propag.*, vol. 58, no. 4, pp. 1202–1213, Apr. 2010.

[20] Y. Wu, Y. Chen, L. Jiao, Y. Liu, and Z. Ghassemlooy, "Dual-band dual-mode substrate integrated waveguide filters with independently reconfigurable TE_{101} resonant mode," *Sci. Rep.*, vol. 6, Aug. 2016, Art. no. 31922.

[21] X.-X. Yang, L. Di, Y. Yu, and S. Gao, "Low-profile frequency-scanned antenna based on substrate integrated waveguide," *IEEE Trans. Antennas Propag.*, vol. 65, no. 4, pp. 2051–2056, Apr. 2017.

[22] L. Cui, W. Wu, and D.-F. Fang, "Printed frequency beam-scanning antenna with flat gain and low sidelobe levels," *IEEE Antennas Wireless Propag. Lett.*, vol. 12, pp. 292–295, 2013.

[23] D.-F. Guan, Q. Zhang, P. You, Z.-B. Yang, Y. Zhou, and S.-W. Yong, "Scanning rate enhancement of leaky-wave antennas using slow-wave substrate integrated waveguide structure," *IEEE Trans. Antennas Propag.*, vol. 66, no. 7, pp. 3747–3751, Jul. 2018.

[24] K.-M. Mak, K.-K. So, H.-W. Lai, and K.-M. Luk, "A magneto-electric dipole leaky-wave antenna for millimeter-wave application," *IEEE Trans. Antennas Propag.*, vol. 65, no. 12, pp. 6395–6402, Dec. 2017.